Progress in Additive Manufacturing
https://doi.org/10.1007/s40964-023-00492-x

FULL RESEARCH ARTICLE

Effects of infill temperature on the tensile properties and warping of 3D-printed polylactic acid

Dario Croccolo[1] · Massimiliano De Agostinis[1] · Stefano Fini[1] · Mattia Mele[1] · Giorgio Olmi[1] · Giampaolo Campana[1]

Received: 25 February 2023 / Accepted: 5 August 2023

Abstract

Although extensive research has been carried out on the effects of temperature on the properties of parts by fused filament fabrication, no study considered the opportunity to use different temperatures and cooling strategies for the contour and the infill region. The purpose of this investigation is to explore such an opportunity through an experimental campaign on polylactic acid. Specifically, the variations in tensile properties and warping occurring with different infill temperatures and cooling methods are documented. The results demonstrate that diversifying process parameters used for the contour and infill of the part allow for significant improvements in mechanical properties without affecting the distortion of the manufactured samples. This result can be achieved by either increasing the nozzle temperature or switching off the cooling fan during infilling.

Keywords Fused filament fabrication · Infill · Temperature · Polylactid acid · 3D printing

Abbreviations

3DP	Three-dimensional printing
AD	Anderson–Darling
AM	Additive manufacturing
ANOVA	Analysis of variance
Adj SS	Adjusted sum of squares
CDP	Contour deposition path
DoE	Design of experiment
DS	Deposition speed
FDM	Fused deposition modelling
FFF	Fused filament fabrication
FLIR	Forward-looking infraRed
FoV	Field of view
ID	Infill density
IDP	Infill deposition path
LT	Layer thickness
MoE	Modulus of elasticity
NT	Nozzle temperature
PBO	Part build orientation
PLA	Polylactic acid
RA	Raster angle
SaB	Strain at break
UTS	Ultimate tensile strength

1 Introduction

Fused filament fabrication (FFF), also known as fused deposition modelling (FDM), is the most familiar additive manufacturing (AM) technology to the overwhelming majority of three-dimensional printing (3DP) users [1]. The main reasons behind this popularity are the low cost and easiness of use of these machines [2–4].

One of the main limitations to the industrial applications of FFF is from the limited mechanical properties of manufactured parts, which are generally far below those of the feedstock polymer [5]. For this reason, a number of experimental studies have been conducted to identify the effect of the process parameters on the resistance of 3D-printed artifacts [6–8]. Recent surveys of the literature in this field [9–12] have emphasized several key parameters that can enhance the mechanical performance of parts produced by FFF. These parameters include the part build orientation (PBO), layer thickness (LT), refill density (ID), raster angle (RA), nozzle temperature (NT) and deposition speed (DS). By manipulating these parameters, it is possible to improve the mechanical properties of FFF parts.

✉ Mattia Mele
mattia.mele@unibo.it

[1] Department of Industrial Engineering (DIN), University of Bologna, Viale del Risorgimento 2, Bologna 40136, Italy

Published online: 25 August 2023

Among the materials used for FFF, polylactic acid (PLA) is undoubtedly one the most widespread, thanks to its manufacturability, affordability and non-toxicity [13, 14]. As a result, considerable effort has been put in by researchers to identify the process parameters which most influence the mechanical performance of 3D-printed PLA [15, 16].

The role of PBO means that parts by FFF are characterized by anisotropic properties, with a loss of resistance along the layering direction (generally identified by the *Z*-axis) [17, 18]. The selection of proper build orientation is thus of paramount relevance to achieve the maximum mechanical performances of the part. Several approaches have been proposed in the literature to find the optimal PBO of parts subjected to complex loads [19, 20].

LT presents a promising avenue for enhancing the mechanical properties of components produced via FFF. In general, decreasing the LT leads to an enhancement in mechanical strength [16, 21, 22], although conflicting findings have been reported in the literature [23]. It is important to note that reducing the layer thickness also results in an increase in printing time, which is a trade-off to consider.

Generally, the toolpath used to build each layer consists of a contour deposition path (CDP) and an infill deposition path (IDP). The role of CDP is to define the external shape of the layer; therefore, maximum accuracy is desired in this region. IDP is intended to provide the component with the required resistance [24, 25].

The strategy used for IDP strongly affects the mechanical properties of parts by FFF [26]. Particularly, the ID, which determines the quantity of material deposited during infilling, is of paramount relevance to determine the final properties of parts. Maximum resistance is achieved when using 100% ID [27, 28]. However, this approach results in increased overall printing time [28]. Existing literature also highlights the pivotal role of the angle between the orientation of deposited lines and the principal stress direction, also known as RA, which is crucial to determine the ultimate tensile strength (UTS), modulus of elasticity (MoE) and strain at break (SaB) of the manufactured parts [29]. Along the deposition direction, the material resistance keeps its maximum value, i.e., that of the feedstock polymer. On the contrary, orthogonally to the deposition direction, the mechanical properties are governed by the adhesion force between adjacent lines [30]. It is well established from a variety of studies that the best mechanical properties are obtained when the load is oriented as the deposited lines (i.e., RA=0°), while minimum values are observed when the load direction is normal to the deposition orientation (i.e., RA=90°) [31–34]. This evidence confirms that the polymer cohesion is always higher than or equal to the adhesion between rasters. Ideally, the material should always be deposited along the principal stress direction. Dedicated algorithms have been proposed to try to adapt the deposition path to the stress map on non-trivial geometries and loading conditions [35]. In traditional FFF, these approaches come to a limit in the case of non-planar stresses since rasters are deposited on a plane [36].

The research on the influence of the process parameters in PLA FFF also highlighted the pivotal role of the NT [10, 37]. NT for PLA FFF can vary between 180 °C and 240 °C [38]. The lower limit is to ensure a proper melting of the polymer, and temperatures above 240 °C may lead to the degradation of the material [39]. The experimental observations report that the UTS, MoE and SaB of PLA specimens increase at higher NT [38, 40–43]. The main reason is that, at higher temperatures, the chain dynamics of the polymer melt are faster and more energy is transmitted to the previously deposited material, which results in a stronger adhesion [39, 44, 45]. One major drawback of high extrusion temperature can be the loss of accuracy due to the lower melt viscosity [43]. The latter can also determine a non-uniform morphology of the extruded material, especially in the case of high feed rates [46].

It is worth highlighting that the non-isothermal nature of the cross-section of the deposited bead is of significant importance in the context of the chosen NT, primarily due to the poor thermal conduction properties of the polymer material. Consequently, this non-isothermal behavior gives rise to a complex flow pattern of the extruded polymer melt, which is heavily influenced by the deposition speed [47]. To predict such intricate phenomena, numerous modeling approaches have been proposed in the existing literature [48]. Additionally, accurate modeling of the deposition dynamics necessitates a thorough characterization of the rheological properties of the polymer, as these properties profoundly impact heat transfer and chain diffusion between adjacent deposition lines [49, 50]. These inter-line interactions, in turn, dictate the adhesive force observed at the macro scale between neighboring raster paths [51, 52]. Hence, an appropriate modeling of the rheological and thermal phenomena is vital for intelligent process parameter selection and guiding the development of novel materials [53]. Moreover, it is crucial to note that the strength between adjacent deposition lines is not solely governed by the characteristics of the polymer melt flow; it also depends on the thermal history of the previously deposited material. The deposited material undergoes multiple re-heating cycles, which are influenced by factors such as part size, geometry, process parameters, and deposition path [54, 55].

During the FFF of PLA, a cooling fan is often used to cool the material in place after deposition. This is intended to limit material leakage under the effect of gravity and drag [56, 57]. Results reported in the literature reveal that the speed of the fan has a significant influence on the tensile properties of the manufactured parts. Specifically, higher fan speed determines

a loss in mechanical properties since it reduces the energy of the polymer melt and, as a result, the adhesion forces [58, 59].

Since the CDP and IDP are characterized by different requirements, the process parameters may be varied in these regions. For instance, default printing profiles in slicing software often prescribe a higher deposition speed for infill and support structures, as the precision requirements for these regions are typically considered to be of lesser importance. While this approach enables time savings during printing, it can have adverse effects on the mechanical properties of the fabricated components [9].

To date, no research has explored the opportunity to use different extrusion temperatures in the CDP and IDP. The studies presented in this section suggest that such an approach could lead to benefits in terms of mechanical performance while preserving the accuracy of manufactured parts.

A difference between contouring and infill NT could be obtained by alternatively heating and cooling the nozzle head. Nonetheless, this approach determines a relevant increase in the overall printing time, as demonstrated by preliminary tests presented in the following sections. A different solution is using a dual-extrusion printer, whose nozzles are equipped with the same material but set at different NTs. This approach allows for considerable time-saving but requires a more complex device and the setting of two profiles. When neither time nor equipment costs are acceptable, a less efficient differentiation of thermal conditions between the CDP and IDP can be achieved by switching off the cooling fan during contouring. This can be done by acting on the G-Code without affecting the building time or adding complexity to the printing device.

It is also worth highlighting that these strategies are not alternative to those previously reviewed in this section, but can be combined to the optimization of other process parameters to achieve the highest mechanical performances.

The present study investigates the effects of varying the IDP temperatures and cooling strategies on the properties of PLA parts produced via FFF. For the scope of this investigation, benchmarks are manufactured varying the NTs and the cooling fan speed used for infilling, while the process parameters of the CDP are maintained constant. The tests are conducted at different RAs to investigate the interactions between IDP temperature and infill direction. The tensile, dimensional, geometrical and mass properties of the manufactured parts are measured and processed by statistical techniques to assess their relations with the processing parameters.

2 Method

2.1 Materials and process

The experimental campaign was conducted on a two-nozzle TL-D3Pro printer by Tenlog ®. PLA filament from Makerbot®was used as a feedstock material. Slicing software Ultimaker Cura 5.1.0®was used to prepare GCode files. No support material was used. Table 1 highlights the factors of the design of experiment (DoE), namely, the nozzle temperature used for infill (T_i), the infill direction (α_i) and the cooling fan speed (v_f). The other processing parameters used for printing are reported in Table 2.

Table 1 Factors of the DoE

Factor	Notation	Levels	Values	Unit
Infill direction	α_i	2	0, 90	°
Nozzle temperature (IDP)	T_i	2	200, 230	$°C$
Cooling fan speed	v_f	2	0–100	%

Table 2 Summary of process parameters

Parameter	Notation	Unit	Value
Infill density	d_i	%	100
Extruder number (CDP)	N_{ec}	–	1
Extruder number (IDP)	N_{ei}	–	2
Nozzle temperature (CDP)	T_c	$°C$	200
Build plate temperature	T_p	°	70
Deposition speed (CDP)	v_c	$\frac{mm}{s}$	30
Deposition speed (IDP)	v_i	$\frac{mm}{s}$	60
Layer height	h_L	mm	0.2
Line width	w_L	mm	0.4
Number of contour lines	n_c	–	2

The infill direction α_i is defined as the angle between the deposited line and the X-axis of the machine. For the sake of clarity, in the following sections, this axis will be included in the sketches of specimens used for testing.

As shown in Table 2, the CDP and IDP are deposited using different extruders. In this way, the CDP and IDP can be deposited at different temperatures without heating and cooling the extruder at each layer. Two extruders are also used when the same temperature applies to all the layers (i.e., $T_i = T_c$)o make the results comparable.

The two levels of the parameter v_f reposted in Table 2 correspond to the fan off and on (at the maximum speed). To switch off the fan only in the IDP, the "search and replace" post-processing function of Cura was used. Specifically, the commands M107 (fan off) and M106 (fan on) were inserted before the comment strings ";TYPE:FILL" and ";TYPE:CONTOUR", respectively.

A full-factorial DoE was used in both the tests presented in Sects. 2.4 and 2.5. The factors of this DoE and related levels are summarized in Table 3. Since the experiment consists of three factors varying on 2 levels, eight combinations of process parameters are used for each test. Each combination is printed in a separate job comprising five replications. As

a result, 40 specimens are printed for each test. Analysis of variance (ANOVA) is then used to quantify the influence of each factor and related interactions on the observed properties.

2.2 Printing time

Preliminary tests were carried out to investigate the effects of printing parameters on the printing time. Specifically, a tensile specimen as those described in Sect. 2.4 was printed under different combinations of IDP NT (T_i) and RA (α_i). The tests were replicated using one or two extruders. In the case of one extruder with $T_i = 230$°C, the nozzle is heated and cooled at each layer when moving from the CDP to the IDP and vice versa.

2.3 Extrusion temperature

To observe the actual temperature of the extruded material, forward-looking infrared (FLIR) images of the filament under different combinations of NT (T_i) and fan speed (v_f) were acquired. A Lepton 3.5 camera with 160 × 120 pixels and 57 ° field of view (FoV) with thermal sensitivity ±0.05 °C was used. The thermal measurements were carried out with a similar approach to that presented by [58]. Specifically, the FLIR camera was blocked in a fixed position with respect to the nozzle and the material was extruded in air. The extrusion speed was set to 2 mm/s, which corresponds to that used for IDP under the process parameters presented in Table 2. Tests were performed at room temperature of 25 °C with 40% humidity.

It is worth highlighting that, as discussed in Sect. 1, the material undergoes complex thermal phenomena during deposition [60, 61]. Therefore, the free extrusion in air does not represent the actual temperature of the deposited polymer. Nonetheless, this measurement permits a comparison between different values of T_i and v_f at the processing parameters used for printing. A more precise modeling of the polymer thermal history is out of the scope of this paper and is left as an area for future studies.

2.4 Tensile tests

Tensile tests were carried out according to the ISO 527-2:2012 standard [62]. This test method is widely adopted in the literature to determine the mechanical properties of parts by FFF. A specimen of Type A as the one shown in Fig. 1 was used for testing. The coordinate system in the figure shows the orientation of the specimen during printing. For the sake of clarity, Fig. 1 includes also a detailed view of the central region of the specimen representing the IDP at different values of α_i.

The width and height of the narrow section of each specimen were measured by means of an Alpa Metrology®digital calliper with an accuracy of ±0.01 mm. The mass of the specimens was measured using a Sartorius AX6202®digital scale with an accuracy of ±0.01g.

Tensile tests were carried out on an Instron Universal testing machine series 5966 equipped with a 10 kN load cell. The strain was measured using an extensometer with a gauge length of 80 mm. The test speed was set to 1 mm/s.

After testing, the fracture surfaces were observed through a ZEISS Stemi 508 stereo microscope.

Table 3 Factors of the full-factorial DoE (5 repetitions)

Factor	Unit	Levels	Values
T_i	(°C)	2	200, 230
α_i	(°)	2	0, 90
v_f	(%)	2	0, 100

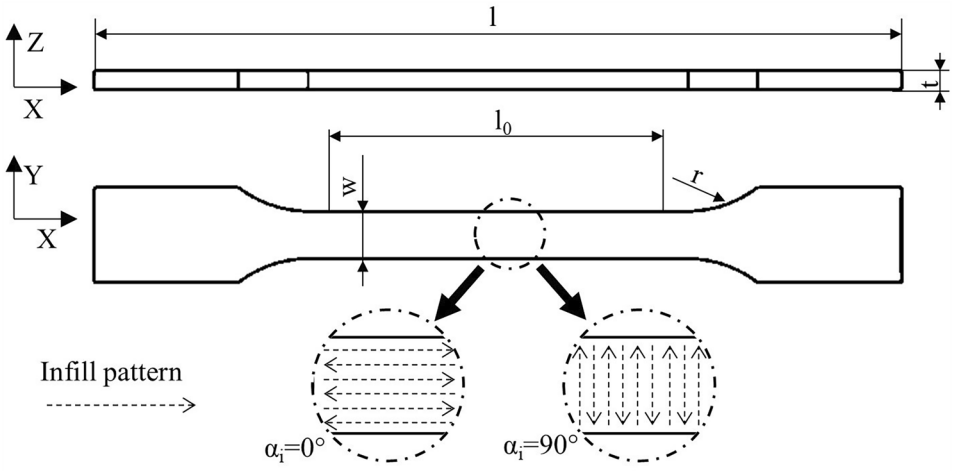

Fig. 1 Tensile test specimen Type A according to ISO 527-2:2012 [62] with a representation of building direction and IDP. Nominal values: l =170 mm, l_0 = 75 mm, w = 10 mm, t = 4 mm, r = 24 mm

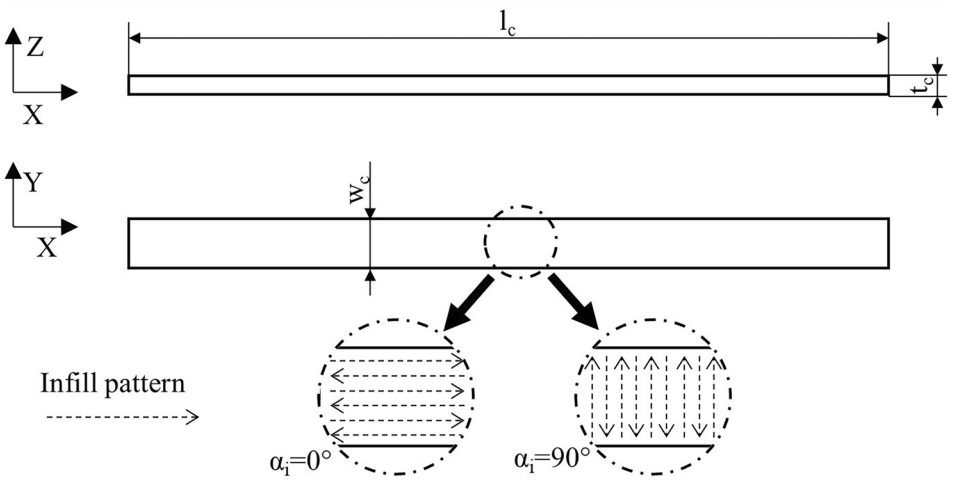

Fig. 2 Specimen for warping measurement [63] with a representation of building direction and IDP. Nominal values: l_c =150 mm, w_c= 10 mm, t_c= 4 mm

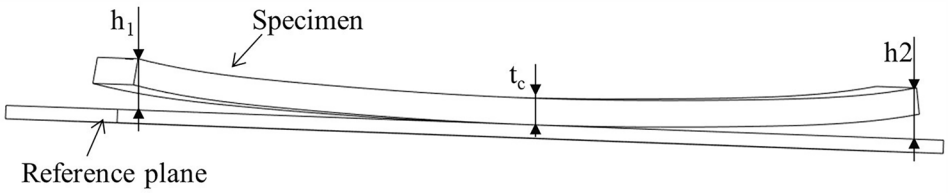

Fig. 3 Graphical representation illustrating the dimensions h_1, h_2, and t that need to be measured to calculate the curling factor f_c

2.5 Warping measurement

The warping of printed parts was measured by means of the method proposed by [63]. To this end, the specimen shown in Fig. 2 is used. The printing orientation and infill pattern are included also in this case to ease understanding.

To quantify the warpage, the printed part was first placed on a flat surface. Then, a calliper was used to measure the distances h_1 and h_2 of the short edges from the surface, and the thickness t_c of the specimen in the central region. These dimensions are schematically shown in Fig. 3. The Alpa Metrology ®digital calliper presented in Sect. 2.4 was used for measuring. The curling factor f_c was finally calculated according to Eq. 1 [63].

$$f_c = \frac{h_1 + h_2}{2} - t_c. \tag{1}$$

3 Results and discussion

3.1 Printing time

Table 4 reports the printing time required to print a single tensile specimen under different combinations of raster angle, printing temperature, and number of extruders.

Table 4 Printing time necessary to manufacture a tensile specimen as shown in Fig. 1

T_i (°C)	α_i (°)	Number of nozzles –	Printing time (min)
200	0	1	50
200	0	2	51
200	90	1	60
200	90	2	61
230	0	1	67
230	0	2	52
230	90	1	77
230	90	2	63

As shown in Table 4, the raster angle plays a crucial role in the printing time, which is higher in the case of $\alpha_i = 90°$. This is well known from previous studies and can be explained considering the higher number of movements [64]. It can also be observed that, in the case of $T_i = 200$ °C, the use of two nozzles has a marginal effect on the printing time, which is increased by one minute regardless of the raster angle. In other words, the adoption of the second nozzle does not determine a significant decrease in the process speed. When two nozzles are used, increasing the temperature of the second nozzle determines an additional building time necessary to heat the extruder at the beginning of the process. Nonetheless, being this time between 1 and 2 min,

its effect on the overall process efficiency can be considered negligible.

The results in Table 4 also show that increasing T_i up to 230 °C when only one nozzle is used determines a rise of 22% and 29% in building time for, respectively, $\alpha_i = 0°$ and $\alpha_i = 90°$. As mentioned above, this is due to the time necessary to heat and cool the nozzle when moving between the contour and infill pattern. Such an increase was considered unacceptable, so this strategy was not included in the following analyses.

3.2 Extrusion temperature

Figure 4 shows the FLIR images of the extrusion under different combinations of NT (T_i) and fan speed (v_f).

By observing Fig. 4, it can be seen that the actual extrusion temperature is remarkably lower than the NT due to the poor thermal conductivity of the polymer. Furthermore, the temperature rapidly decreases as the filament moves from the nozzle. These observations are in line with the findings reported by previous studies [58].

The comparison between Fig. 4a, b reveals that an increase of 30 °C in NT corresponds to an increase of approximately 14 °C in the temperature of the polymer at the nozzle exit.

Figure 4c, d shows that the adoption of the cooling fan determines a decrease in polymer temperature nearby the nozzle slightly higher than 8 °C. This result confirms that the variation of v_f is less effective than that of T_i on the actual temperature of the deposited material.

3.3 Tensile tests

Table 5 summarizes the dimensional and mass properties of the specimens used for tensile tests. The raw data are reported in Table A1 in Appendix A.

Data in Table 5 shows that the average mass of printed specimens varies between 11.55 and 11.89 g. Table 6 shows the results of ANOVA on m measurements. Specifically, the adjusted sum of squares (Adj SS), F value and p value are reported [65]. To verify the hypothesis beneath ANOVA, the Anderson–Darling (AD) test was performed to verify the normality of standardized residuals. This test resulted in a p value equal to 0.162, which allows for rejecting the hypothesis of non-normal distribution and validating the results of the ANOVA.

The results reported in Table 6 show that all p values are less than 0.05, i.e., all the factors are significant for the specimen mass. The influence of each factor can be seen in the main effect plot shown in Fig. 5.

The infill orientation appears to be the most influential factor. This finding can be explained if considering that, due to the shape of the specimen (shown in Fig. 1) the hatching strategy determines a non-complete infill of the part.

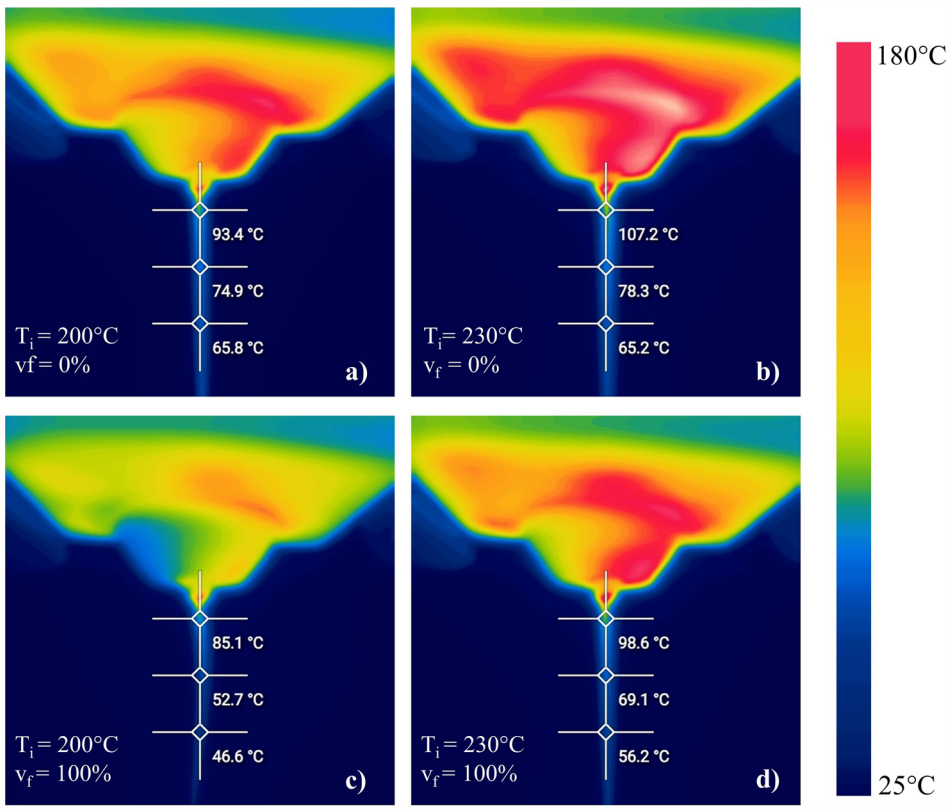

Fig. 4 FLIR images of the extruded filament at a) $T_i = 200$ °C and $v_f = 0\%$, b) $T_i = 230$ °C and $v_f = 0\%$, c) $T_i = 200$ °C and $v_f = 100\%$, d) $T_i = 230$ °C and $v_f = 100\%$

Table 5 Mass and dimensional properties of tensile specimens

T_i (°C)	α_i (°)	v_f (%)	m (g)	t (mm)	w (mm)
200	0	0	11.55 ± 0.02	3.95 ± 0.02	10.30 ± 0.09
200	0	100	11.55 ± 0.03	3.97 ± 0.01	10.32 ± 0.10
200	90	0	11.72 ± 0.01	4.01 ± 0.02	10.45 ± 0.13
200	90	100	11.72 ± 0.02	4.06 ± 0.03	10.41 ± 0.07
230	0	0	11.72 ± 0.01	4.03 ± 0.01	10.39 ± 0.12
230	0	100	11.66 ± 0.02	4.06 ± 0.04	10.37 ± 0.10
230	90	0	11.81 ± 0.02	3.99 ± 0.01	10.32 ± 0.02
230	90	100	11.79 ± 0.02	4.00 ± 0.02	10.40 ± 0.05

Table 6 Results of ANOVA for specimens' mass (m)

Factor	Adj SS	F value	p value
T_i(°C)	0.121	273	$< 10^{-3}$
α_i(°)	0.196	442	$< 10^{-3}$
v_f(%)	0.004	9.02	0.005
$T_i \times \alpha_i$(°C×°)	0.0084	18.96	$< 10^{-3}$
$T_i \times v_f$(°C)	0.006	14.09	0.001
$v_f \times \alpha_i$(°)	0.00120	2.73	0.108
$T_i \times v_f \times \alpha_i$(°)	0.000999	2.35	0.1354

In particular, the 90° infill strategy allows for a more dense volume infill at the fillet. This is confirmed by the nominal volume of filament deposited for each specimen calculated by the slicing software, which is equal to 9,758 mm^3 for $\alpha_i = 0°$ and equal to 9,858 mm^3 when $\alpha_i = 90°$.

Table 6 also shows a relevant effect of the printing temperature. As shown in Fig. 5, the higher temperature determines an increase in part mass. The same result was reported, for example, by Kuznetsov et al. [59], who attributed the higher mass to the lower extrusion resistance at higher temperatures, which yields a more efficient feeding of the filament. Possibly, the fan speed determines a similar phenomenon but with a less intense effect, as can be seen by the higher p value (and lower F value) in Table 6.

As reported in Table 6, a significant influence of interactions between T_i and both other factors (namely v_f and α_i) is observed. These effects can be seen in the interaction plot shown in Fig. 6.

As shown in Fig. 6, the increase in mass due to infill temperature is more relevant when $\alpha_i = 90°$. This suggests that the higher material flow, as an effect of incremented temperatures, partially compensates for voids due to the radius infilling discussed above. The plot of interactions between T_i and v_f highlights that the effect of fan speed on the part mass is significant at 230 °C, while it becomes almost negligible at 200 °C.

No correlation between the varied factors and the dimensions of the transversal section (w and s) can be observed. This finding is of great relevance since it proves that the variations in the infill temperature and cooling strategy do not negatively affect the dimensional accuracy of the printed parts.

The results of tensile tests are reported in Table 7. The specimens exhibited a predominantly brittle fracture, in line with the results presented by previous literature on this material [46]. It is worth mentioning that several specimens exhibited fracture at the limit of the gauge length. Arguably, this is also due to the non-complete filling of the fillets mentioned above. This limitation of the specimen used for testing has been experienced also by previous studies [66]

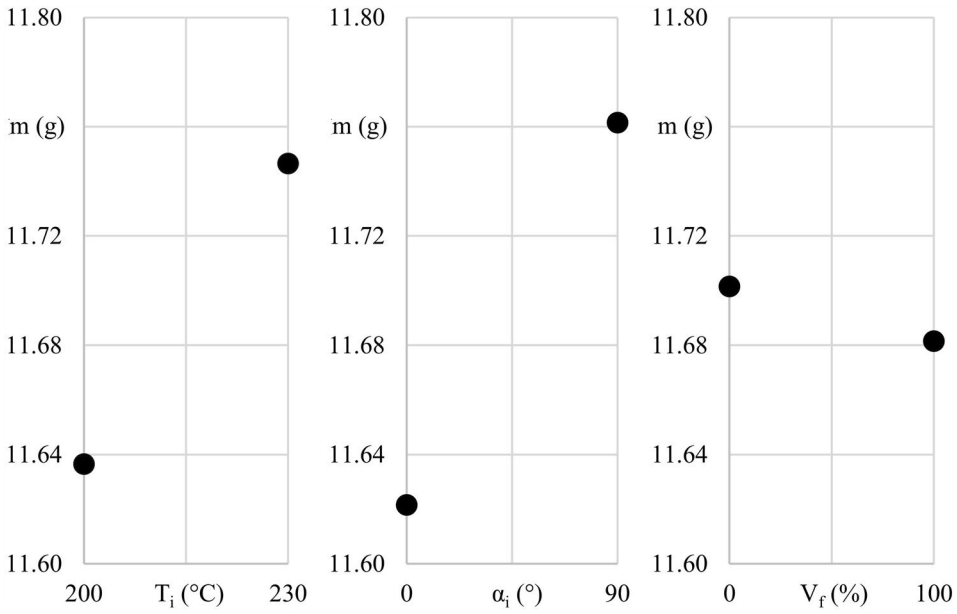

Fig. 5 Main effect plots illustrating the influences of IDP T_i, infill direction α_i and cooling fan speed v_f on the mass of the specimen m

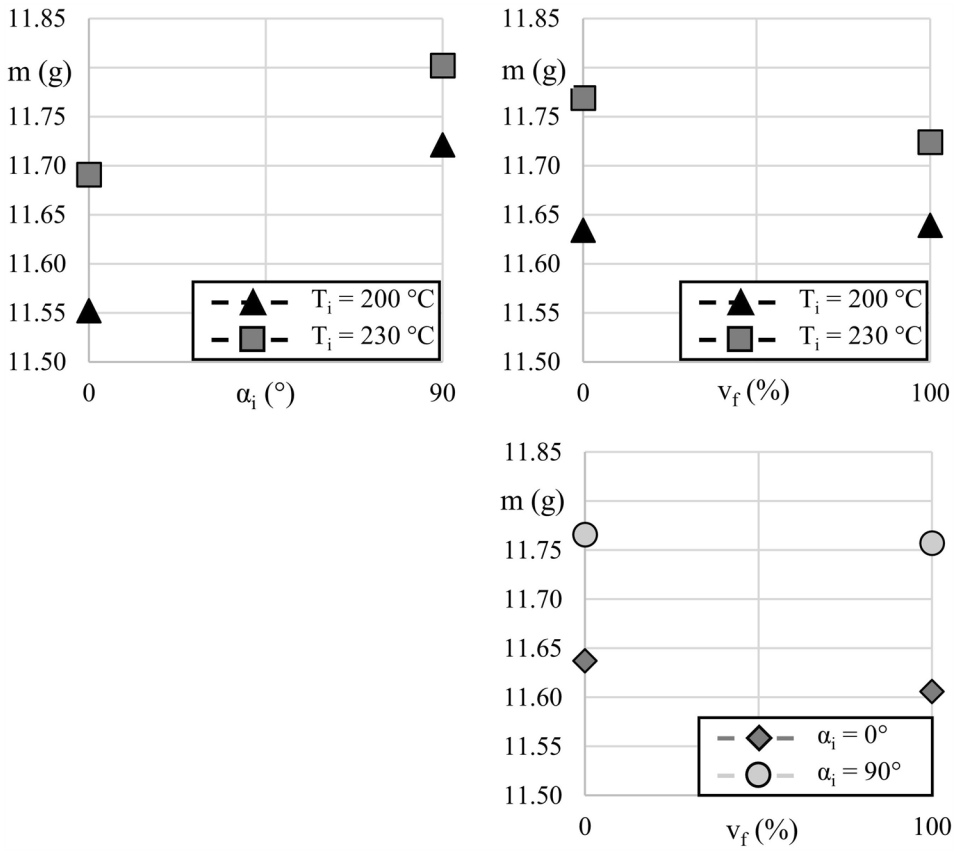

Fig. 6 Interaction plots illustrating the combined effects of IDP T_i, infill direction α_i and cooling fan speed v_f on the mass of the specimen m

Table 7 Mechanical properties of tensile specimens

T_i (°C)	α_i (°)	v_f (%)	UTS (MPa)	SaB (mm/mm)	MoE (MPa)
200	0	0	59.6 ± 2.4	0.016 ± 0.001	3439 ± 62
200	0	100	56.5 ± 3.2	0.017 ± 0.002	3397 ± 159
200	90	0	54.6 ± 1.2	0.024 ± 0.001	3290 ± 97
200	90	100	53.1 ± 1.4	0.022 ± 0.001	3236 ± 47
230	0	0	61.5 ± 1.5	0.019 ± 0.001	3273 ± 40
230	0	100	60.1 ± 1.8	0.023 ± 0.002	3313 ± 68
230	90	0	59.6 ± 0.6	0.025 ± 0.004	3312 ± 205
230	90	100	57.4 ± 1.1	0.019 ± 0.001	3347 ± 57

and underlines the need for a specific standard for tensile tests on polymers by FFF [17].

ANOVA was performed on the UTS data to investigate the influence of each experimental factor. The results of this analysis are reported in Table 8. AD test on standardized residuals led to p-value=0.253, which allows for validating the results of ANOVA. The main effect plot shown in Fig. 7 gives an insight into the effect of each factor on the part resistance.

Firstly, it is possible to highlight the significant role of the infill direction on the UTS. This expected result is in accordance with the vast body of the literature on FFF. It is well-established that the cohesive force within the polymer is higher than the adhesive force between adjacent beads [7, 16, 30].

Table 8 Results of ANOVA for UTS (MPa)

Factor	Adj SS	F value	p value
T_i(°C)	136	33.6	$< 10^{-3}$
α_i(°)	1.07×10^2	26.3	$< 10^{-3}$
v_f(%)	4.14×10	10.2	0.003
$T_i \times \alpha_i$(°C×°)	8.82	2.13	0.154
$T_i \times v_f$(°C)	0.77	0.19	0.669
$v_f \times \alpha_i$(°)	0.240	0.06	0.811
$T_i \times v_f \times \alpha_i$(°)	3.3145	0.80	0.379

Results in Table 8 show that the deposition temperature of the infill T_i is the most influential factor. Particularly, as shown in Fig. 7, the UTS of specimens increases when higher nozzle temperatures are used. This finding is in line with results reported in the body of literature when the deposition temperature of the whole part is varied [39, 59]. As mentioned in Sect. 1, this can be explained considering the different rheological behavior of the material, which promotes the bonding between adjacent lines [53, 54].

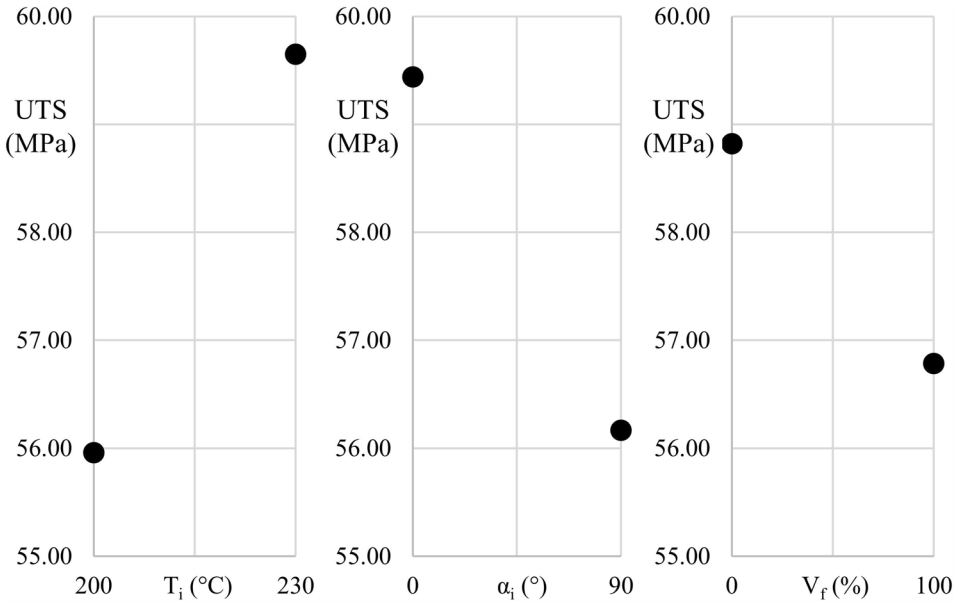

Fig. 7 Main effect plots illustrating the influences of IDP T_i, infill direction α_i and cooling fan speed v_f on the UTS of the specimen

It can also be observed that the decrease in polymer viscosity at higher temperatures determines a better diffusion of extruded PLA on the underlying layer and a reduction of voids between rasters [45, 48, 67]. This is confirmed by comparing the microscopical observations shown in Fig. 8a, b, where the fracture region of specimens printed at $T_i = 200$ °C and $T_i = 230$ °C, respectively, are shown. By observing Fig. 8a, a clear separation between layers can be observed in the case of $T_i = 200$ °C. Moreover, it is possible to clearly distinguish the cross section of the different deposition lines. On the other hand, when $T_i = 230$ °C, the fracture region appears as a compact surface, as can be seen in Fig. 8b. It is worth remarking that, unlike in previous studies, this result has been achieved by varying only the temperature of the infill pattern.

It must be highlighted that the results of the ANOVA in Table 8 yield a p value lower than 0.05 for v_f. This evidence, combined with the trend shown in Fig. 7, allows for concluding that the switch-off of the cooling fan during the infill has also a beneficial influence on the mechanical resistance of manufactured parts. The reason behind this phenomenon is analogous to that presented above discussing the influence of T_i. The absence of forced cooling leads to a higher temperature of the deposited material, which in turn results in a more effective bonding between layers and adjacent lines. This outcome can also be seen by comparing the microscopic observation of the fracture region shown in Fig. 9 ($T_i = 200$ °C, $v_f = 0\%$, $\alpha_i = 0°$) with the one in Fig. 8a ($T_i = 200$ °C, $v_f = 100\%$, $\alpha_i = 0°$). This comparison demonstrates that a more compact surface is achieved without the use of cooling fan. On the other hand, comparing Figs. 8b and 9, it is possible to notice that the improvement in material adhesion is less

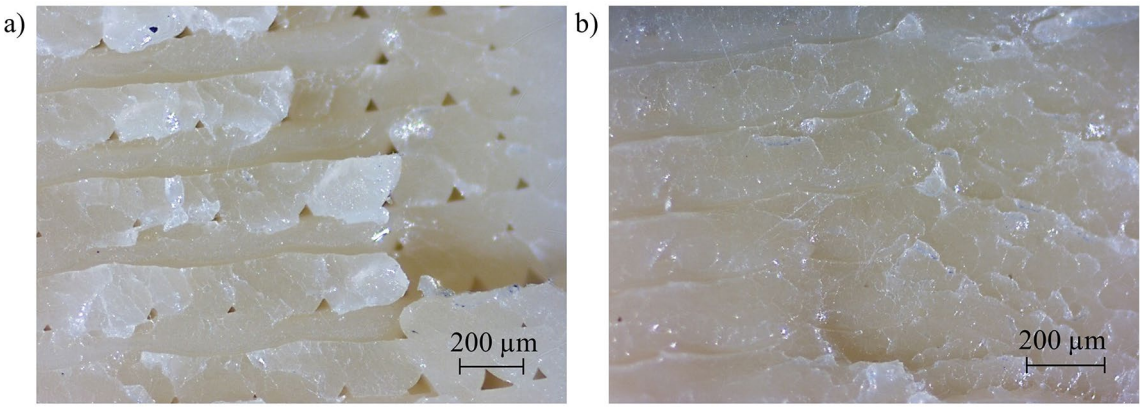

Fig. 8 Stereoscopic observation of the fracture region for specimen printed at **a** $T_i = 200$ °C and **b** $T_i = 230$ °C. ($v_f = 100\%$, $\alpha_i = 0°$)

than that achieved by increasing the nozzle temperature. This is confirmed by the lower F value reported in Table 8.

This result is consistent with the findings of Lee and Liu [58]. It is worth remarking that, unlike in that work, in this study, the improvement in mechanical resistance is achieved by switching off the fan only during the infill. This allows for better control of the contour lines, which directly affect the accuracy of manufactured parts.

On the other hand, an opposite trend was observed by Tan et al. [68] in the case of recycled PLA. As discussed by the authors of that study, this is arguably due to the differences in material properties between virgin and recycled feedstock polymer.

The results of ANOVA presented in Table 8 show that all the p values of second-order and third-order terms are higher than 0.05. This finding highlights that the interactions between experimental factors are not significant to UTS. Consequently, the interaction plots of the ANOVA are not reported. An important outcome is that the aforementioned conclusions regarding the beneficial effects of infill deposition temperature and infill cooling fan switch-off keep valid regardless of the selected infill pattern.

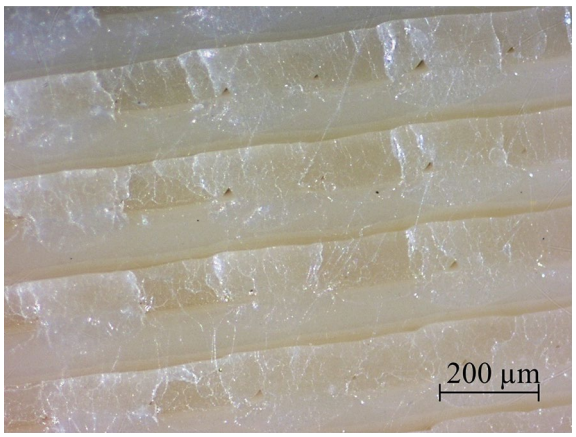

Fig. 9 Stereoscopic observation of the fracture region for specimen printed at $T_i = 200$ °C, $v_f = 0\%$, $\alpha_i = 0°$)

As far as the SaB is concerned, the results are affected by the only infill direction, being higher when $\alpha_i = 0°$. This result is consistent with findings in the literature [69]. On the contrary, no statistically significant correlation between SaB and T_i or v_f was found. It is thus possible to conclude that the strategies proposed in this study do not affect the elongation at break of the printed parts.

3.4 Warping

Table 9 summarizes the result of measurements on the warping specimens described in Sect. 2.5. The raw data are reported in Table A2 in Appendix A. The height values h_1 and h_2, and the thickness t_c (see Fig. 2) are reported. The curling factor f_c calculated as by Eq. 1 is also given.

An ANOVA was performed on f_c values to determine the influential factors. The results of this analysis are reported in Table 10. The AD test of standardized residuals returned a p value equal to 0.507, which allows for accepting the analysis results.

The results of ANOVA suggest that the infill orientation is the only relevant factor as far as warping is concerned. Specifically, higher deformations are observed for $\alpha_i = 0°$. This can be explained if considering that the internal stress of the material is more severe within deposited lines due to the higher material density.

No connection between the curling factor and the temperature-related factors, namely T_i and v_f, is observed. On the other hand, a significant effect of interactions between T_i and α_i, and between T_i and v_f is observed.

The interaction plot in Fig. 10 shows a significant difference between the influence of the raster orientation at $T_i = 200$ °C and $T_i = 230$ °C. Specifically, the adoption of $\alpha_i = 90°$ leads to a sharp reduction in warping at a lower temperature, while is almost negligible at $T_i = 230$ °C. A possible explanation of this behavior is that lower infill temperatures determine a worse adhesion between the building plate and the specimen. This may magnify the effect of orientation on internal stresses discussed above.

Table 9 Results of warping measurements

T_i(°C) (°C)	α_i (°)	v_f(%) (%)	h_1 (mm)	h_2 (mm)	t_c (mm)	f_c (mm)
200	90	0	7.2 ± 0.01	3.96 ± 0.01	3.95 ± 0.01	3.95 ± 0.01
200	0	0	7.1 ± 0.03	3.99 ± 0.03	4.2 ± 0.06	4.23 ± 0.04
200	0	100	7 ± 0.02	4.02 ± 0.02	4.78 ± 0.18	4.74 ± 0.09
200	90	100	7.2 ± 0.02	4.03 ± 0.03	4 ± 0.03	4 ± 0.03
230	0	100	7.1 ± 0.02	4.09 ± 0.03	4.13 ± 0.11	4.1 ± 0.08
230	90	0	7.1 ± 0.01	4.09 ± 0.02	4.3 ± 0.07	4.31 ± 0.02
230	0	0	7.1 ± 0.02	4.05 ± 0.02	4.49 ± 0.06	4.47 ± 0.09
230	90	100	6.9 ± 0.08	3.96 ± 0	4.06 ± 0.07	4.11 ± 0.04

Table 10 Results of ANOVA for curling factor f_c

Factor	Adj SS	F-value	p-value
$T_i(°C)$	0.008	0.43	0.516
$\alpha_i(°)$	0.712	38.52	$< 10^{-3}$
$v_f(\%)$	0.000	0.01	0.922
$T_i \times \alpha_i(°C\times°)$	0.549	29.70	$< 10^{-3}$
$T_i \times v_f(°C)$	0.530	28.70	$< 10^{-3}$
$v_f \times \alpha_i(°)$	0.0158	0.86	0.362
$T_i \times v_f \times \alpha_i(°)$	0.00095	0.20	0.6561

A crossover strong interaction is observed between T_i and v_f. Specifically, at lower infill temperature, namely $T_i = 200$ °C, the forced cooling ($v_f = 100\%$) determines an increase in the curling factor. This is probably due to a worse adhesion of the material to the build plate, as discussed above. On the other hand, when higher temperature is considered, i.e., $T_i = 200$ °C, the cooling fan has a beneficial influence on the part warping. A possible explanation is that, at this temperature, the linear thermal contraction of the polymer is more relevant than adhesion. Therefore, switching off the fan induces a higher thermal gradient between the first and the last layer, which in turn determines higher internal stress and distortion.

4 Conclusions

This paper presented a novel approach to enhance the mechanical properties of parts manufactured using fused filament fabrication by manipulating the process parameters of the infill deposition pattern. Specifically, the impact of nozzle temperature and cooling fan speed on the printed parts was investigated.

To vary the temperature of the infill lines, a second extruder was employed in this study. Preliminary tests revealed that this method resulted in a negligible increase in printing time. However, it is important to note that this technique can only be applied to machines equipped with two extruders. Conversely, adjusting the speed of the cooling fan during the infill deposition did not introduce any additional complexity or processing time. Thermal analysis demonstrated that deactivating the cooling fan led to a substantial rise in the temperature of the extruded filament.

Tensile testing of the printed parts demonstrated that using a higher temperature for the infill pattern significantly increased the ultimate tensile strength of the components. Moreover, improvements in mechanical properties were observed when keeping the nozzle temperature constant and varying the cooling fan speed during infill deposition.

Importantly, the enhancement in mechanical properties was achieved without compromising the dimensional

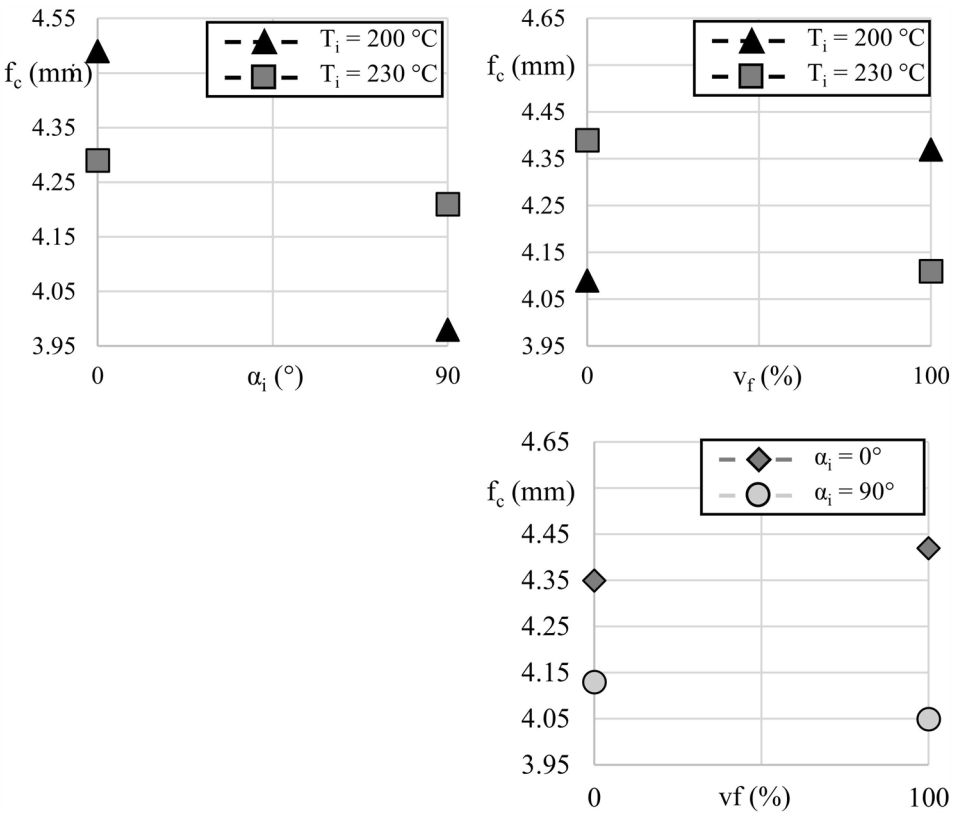

Fig. 10 Interaction plots illustrating the combined effects of IDP T_i, infill direction α_i and cooling fan speed v_f on the curling factor f_c

accuracy of the parts, which is primarily influenced by the contouring process parameters. Warping tests revealed that the out-of-plane deformation of the parts was predominantly influenced by the raster orientation. The impact of the cooling strategy on warping was found to be dependent on the infill temperature, with build plate adhesion playing a significant role in this regard.

Overall, the results of this study clearly demonstrate that the ultimate tensile strength of PLA parts produced by fused filament fabrication can be enhanced by adjusting the infill processing parameters, while maintaining dimensional and geometrical accuracy. This practical and easily applicable strategy offers a means to improve the mechanical strength of 3D-printed components. Future investigations will focus on evaluating the effects of this deposition strategy on the impact toughness of printed parts.

Appendix A: Raw data

See Tables 11 and 12.

Table 11 Results of tensile tests

Test	T_i (°C)	α_i (°)	v_f (%)	m (g)	t (mm)	w (mm)	UTS (MPa)	SaB (mm/mm)	MoE (MPa)
1	230	0	100	11.64	4.11	10.37	61.5	0.024	3296
2	230	0	100	11.68	4	10.41	61.9	0.023	3440
3	230	0	100	11.64	4.03	10.22	57.5	0.02	3310
4	230	0	100	11.67	4.06	10.53	58.4	0.022	3281
5	230	0	100	11.66	4.11	10.33	61.4	0.023	3237
6	230	90	100	11.82	4.02	10.49	57.4	0.02	3313
7	230	90	100	11.76	4	10.39	56.9	0.02	3342
8	230	90	100	11.78	3.98	10.41	55.8	0.017	3349
9	230	90	100	11.79	4.02	10.32	57.7	0.018	3279
10	230	90	100	11.8	3.97	10.38	59.2	0.02	3450
11	200	90	100	11.73	4.08	10.33	54.7	0.023	3255
12	200	90	100	11.72	4	10.5	51.2	0.021	3281
13	200	90	100	11.69	4.09	10.47	52.2	0.02	3245
14	200	90	100	11.74	4.08	10.4	52.5	0.022	3146
15	200	90	100	11.74	4.03	10.35	54.7	0.023	3255
16	200	0	100	11.55	3.96	10.41	60	0.021	3311
17	200	0	100	11.54	3.98	10.35	56.6	0.016	3226
18	200	0	100	11.56	3.98	10.13	58.5	0.016	3337
19	200	0	100	11.6	3.97	10.4	50.7	0.014	3687
20	200	0	100	11.52	3.98	10.29	57	0.018	3426
21	200	0	0	11.55	3.96	10.26	61.4	0.017	3414
22	200	0	0	11.56	3.94	10.42	60.5	0.018	3531
23	200	0	0	11.57	3.92	10.38	59.2	0.015	3429
24	200	0	0	11.55	3.98	10.16	55.1	0.015	3347
25	200	0	0	11.52	3.95	10.26	61.8	0.017	3476
26	230	0	0	11.72	4.04	10.44	62.9	0.02	3229
27	230	0	0	11.74	4.03	10.47	59.7	0.019	3310
28	230	0	0	11.72	4.02	10.34	63.5	0.019	3317
29	230	0	0	11.71	4.05	10.18	60.4	0.018	3287
30	230	0	0	11.73	4.02	10.54	60.9	0.019	3221
31	200	90	0	11.73	4.05	10.29	53.6	0.025	3282
32	200	90	0	11.71	3.99	10.43	56.7	0.026	3422
33	200	90	0	11.72	4.01	10.48	53.6	0.025	3357
34	200	90	0	11.7	4.01	10.37	54	0.023	3133
35	200	90	0	11.73	4.01	10.68	55.3	0.023	3257
36	230	90	0	11.85	4.01	10.31	60.1	0.021	3459
37	230	90	0	11.79	3.98	10.33	58.7	0.02	3560
38	230	90	0	11.8	4	10.35	59.8	0.033	3247
39	230	90	0	11.8	3.98	10.31	58.9	0.024	2963
40	230	90	0	11.83	4	10.29	60.2	0.025	3329

Table 12 Results of warping tests

Test	T_i ($°C$)	α_i (°)	v_f %	t_c (mm)	h_1 (mm)	h_2 (mm)	f_c (mm)
1	200	90	0	3.94	3.95	3.98	0.025
2	200	90	0	3.97	3.96	3.95	−0.015
3	200	90	0	3.97	3.96	3.94	−0.02
4	200	90	0	3.97	3.95	3.99	0
5	200	90	0	3.96	3.94	3.92	−0.03
6	200	0	0	4.02	4.18	4.28	0.21
7	200	0	0	3.94	4.25	4.24	0.305
8	200	0	0	3.99	4.23	4.25	0.25
9	200	0	0	4	4.1	4.23	0.165
10	200	0	0	4.02	4.24	4.33	0.265
11	200	0	100	3.99	4.54	5.15	0.855
12	200	0	100	4.05	4.99	4.47	0.68
13	200	0	100	4.02	5	4.67	0.815
14	200	0	100	4.03	4.73	4.55	0.61
15	200	0	100	4.01	4.65	4.64	0.635
16	200	90	100	4	4	3.96	−0.02
17	200	90	100	4.02	3.96	3.96	−0.06
18	200	90	100	4.03	3.98	4.03	−0.025
19	200	90	100	4.08	4.04	4.03	−0.045
20	200	90	100	4.04	4	4.02	−0.03
21	230	0	100	4.1	4.33	4.19	0.16
22	230	0	100	4.08	4.08	4.08	0
23	230	0	100	4.12	4.05	4.01	−0.09
24	230	0	100	4.04	4.07	4.11	0.05
25	230	0	100	4.12	4.05	4.06	−0.06
26	230	90	0	4.09	4.33	4.34	0.245
27	230	90	0	4.09	4.31	4.32	0.225
28	230	90	0	4.07	4.33	4.26	0.225
29	230	90	0	4.12	4.36	4.27	0.195
30	230	90	0	4.09	4.17	4.37	0.18
31	230	0	0	4.04	4.42	4.53	0.435
32	230	0	0	4.06	4.49	4.29	0.33
33	230	0	0	4.06	4.44	4.31	0.315
34	230	0	0	4.07	4.6	4.65	0.555
35	230	0	0	4.01	4.51	4.45	0.47
36	230	90	100	3.96	4.08	4.16	0.16
37	230	90	100	3.96	4.17	4.16	0.205
38	230	90	100	3.95	4.08	4.17	0.175
39	230	90	100	3.95	3.99	4.15	0.12
40	230	90	100	3.96	3.99	4.15	0.11

Acknowledgements Financed by the European Union - NextGenerationEU (National Sustainable Mobility Center CN00000023, Italian Ministry of University and Research Decree n. 1033-17/06/2022, Spoke 11-Innovative Materials & Lightweighting). The opinions expressed are those of the authors only and should not be considered as representative of the European Union or the European Commission's official position. Neither the European Union nor the European Commission can be held responsible for them. The authors would like to thank Mr. Marco Lia for his support.

Funding Open access funding provided by Alma Mater Studiorum - Università di Bologna within the CRUI-CARE Agreement.

Data availability The authors confirm that the data supporting the findings of this study are available within the article.

Declarations

Conflict of interest The authors declare that they have no known competing financial interests or personal relationships that could have appeared to influence the work reported in this paper.

References

1. Sculpteo (2022) The state of 3D printing 2022, 23
2. Shahrubudin N, Lee TC, Ramlan R (2019) An overview on 3D printing technology: technological, materials, and applications. Proc Manuf 35:1286–1296. https://doi.org/10.1016/j.promfg.2019.06.089
3. Kishore K, Sinha MK (2021) A state-of-the-art review on fused deposition modelling process, pp. 855–864. https://doi.org/10.1007/978-981-15-8542-5_24
4. Ciotti M, Campana G, Mele M (2022) A review of the accuracy of thermoplastic polymeric parts fabricated by additive manufacturing. Rapid Prototyp J 28(2):358–389. https://doi.org/10.1108/RPJ-11-2020-0295
5. Zhang P, Wang Z, Li J, Li X, Cheng L (2020) From materials to devices using fused deposition modeling: a state-of-art review. Nanotechnol Rev 9(1):1594–1609. https://doi.org/10.1515/ntrev-2020-0101
6. Tran TQ, Ng FL, Kai JTY, Feih S, Nai MLS (2022) Tensile strength enhancement of fused filament fabrication printed parts: a review of process improvement approaches and respective impact. Addit Manuf 54:102724. https://doi.org/10.1016/j.addma.2022.102724
7. Nyiranzeyimana G, Mutua JM, Mose BR, Mbuya TO (2021) Optimization of process parameters in fused deposition modelling of thermoplastics: A review. Materialwiss Werkstofftech 52(6):682–694. https://doi.org/10.1002/mawe.202000193
8. Doshi M, Mahale A, Singh SK, Deshmukh S (2021) Printing parameters and materials affecting mechanical properties of FDM-3D printed Parts: Perspective and prospects. Materials Today: Proceedings 50:2269–2275. https://doi.org/10.1016/j.matpr.2021.10.003
9. Gao G, Xu F, Xu J, Tang G, Liu Z (2022) A survey of the influence of process parameters on mechanical properties of fused deposition modeling parts. MDPI. https://doi.org/10.3390/mi13040553
10. Mengesha Medibew T (2022) A comprehensive review on the optimization of the fused deposition modeling process parameter for better tensile strength of PLA-printed parts. Adva Mater Sci Eng 2022(2):2. https://doi.org/10.1155/2022/5490831
11. Singh A, Shukla A, Singh A, Deep Singh A, Kumar Arora P (2022) Review on Process Parameters of FDM and Their Impact on Tensile Strength and Wear Resistance of Additive Manufacturing Specimen. In: Advances in Transdisciplinary Engineering, vol. 27, pp. 274–279. IOS Press BV, ???. https://doi.org/10.3233/ATDE220753
12. Syrlybayev D, Zharylkassyn B, Seisekulova A, Akhmetov M, Perveen A, Talamona D (2021) Optimisation of strength properties of FDM printed parts-A critical review. MDPI AG. https://doi.org/10.3390/polym13101587
13. Liu Z, Wang Y, Wu B, Cui C, Guo Y, Yan C (2019) A critical review of fused deposition modeling 3D printing technology in manufacturing polylactic acid parts. Int J Adv Manuf Technol 102(9–12):2877–2889. https://doi.org/10.1007/s00170-019-03332-x
14. Blaj M, Oancea G (2021) Fused deposition modelling process: A literature review. IOP Conference Series: Materials Science and Engineering **1009**(1). https://doi.org/10.1088/1757-899X/1009/1/012006
15. Luzanin O, Movrin D, Stathopoulos V, Pandis P, Radusin T, Guduric V (2019) Impact of processing parameters on tensile strength, in-process crystallinity and mesostructure in FDM-fabricated PLA specimens. Rapid Prototyp J 25(8):1398–1410. https://doi.org/10.1108/RPJ-12-2018-0316
16. Cojocaru V, Frunzaverde D, Miclosina CO, Marginean G (2022) The influence of the process parameters on the mechanical properties of PLA specimens produced by fused filament fabrication-a review. Polymers 14:5. https://doi.org/10.3390/polym14050886
17. Gordelier TJ, Thies PR, Turner L, Johanning L (2019) Optimising the FDM additive manufacturing process to achieve maximum tensile strength: a state-of-the-art review. Rapid Prototyp J 25(6):953–971. https://doi.org/10.1108/RPJ-07-2018-0183
18. Chacón JM, Caminero MA, García-Plaza E, Núñez PJ (2017) Additive manufacturing of PLA structures using fused deposition modelling: effect of process parameters on mechanical properties and their optimal selection. Mater Des 124:143–157. https://doi.org/10.1016/j.matdes.2017.03.065
19. Birosz MT, Safranyik F, Andó M (2022) Build orientation optimization of additive manufactured parts for better mechanical performance by utilizing the principal stress directions. J Manuf Process 84:1094–1102. https://doi.org/10.1016/j.jmapro.2022.10.038
20. Sheng H, Xu J, Zhang S, Tan J (2022) Build orientation optimization for extrusion-based additive manufacturing coupling with adaptive slicing. Int J Adv Manuf Technol 123(3–4):1133–1158. https://doi.org/10.1007/s00170-022-10237-9
21. Garzon-Hernandez S, Garcia-Gonzalez D, Jérusalem A, Arias A (2020) Design of FDM 3D printed polymers: An experimental-modelling methodology for the prediction of mechanical properties. Mater Des 188:108414. https://doi.org/10.1016/j.matdes.2019.108414
22. Srivastava M, Maheshwari S, Kundra T, Rathee S (2017) Multi-response optimization of fused deposition modelling process parameters of ABS using response surface methodology (RSM)-based desirability analysis. Mater Today: Proc 4(2):1972–1977. https://doi.org/10.1016/j.matpr.2017.02.043
23. Farashi S, Vafaee F (2022) Effect of printing parameters on the tensile strength of FDM 3D samples: a meta-analysis focusing on layer thickness and sample orientation. Progr Addit Manuf 7(4):565–582. https://doi.org/10.1007/s40964-021-00247-6
24. Gibson I, Rosen D, Stucker B, Khorasani M (2021) Additive Manufacturing Technologies, pp. 1–459. Springer, Boston, MA. https://doi.org/10.1007/978-3-030-56127-7. https://www.springer.com/in/book/9783030561260
25. Redwood B, Schöffer F, Garret B (2017) The 3D Printing Handbook. 3D Hubs, 304

26. Kehinde Aworinde A, Oluropo Adeosun S, Adekunle Oyawale F, Titilayo Akinlabi E, Akinlabi SA (2019) Parametric effects of fused deposition modelling on the mechanical properties of polylactide composites: a review. J Phys: Conf Ser 1378(2):10. https://doi.org/10.1088/1742-6596/1378/2/022060
27. Gomez-Gras G, Jerez-Mesa R, Travieso-Rodriguez JA, Lluma-Fuentes J (2018) Fatigue performance of fused filament fabrication PLA specimens. Mater Des 140:278–285. https://doi.org/10.1016/j.matdes.2017.11.072
28. Alvarez CKL, Lagos CRF, Aizpun M (2016) Investigating the influence of infill percentage on the mechanical properties of fused deposition modelled ABS parts. Ingenieria e Investigacion 36(3):110–116. https://doi.org/10.15446/ing.investig.v36n3.56610
29. Letcher T, Behzad R, Sina J (2015) Experimental Study of Mechanical Properties of Additively. Proceedings of the ASME 2015 International Mechanical Engineering Congress and Exposition IMECE2015, 1–8
30. Croccolo D, De Agostinis M, Olmi G (2013) Experimental characterization and analytical modelling of the mechanical behaviour of fused deposition processed parts made of ABS-M30. Comput Mater Sci 79:506–518. https://doi.org/10.1016/j.commatsci.2013.06.041
31. Afrose MF, Masood SH, Iovenitti P, Nikzad M, Sbarski I (2016) Effects of part build orientations on fatigue behaviour of FDM-processed PLA material. Progr Addit Manuf 1(1–2):21–28. https://doi.org/10.1007/s40964-015-0002-3
32. Tymrak BM, Kreiger M, Pearce JM (2014) Mechanical properties of components fabricated with open-source 3-D printers under realistic environmental conditions. Mater Des 58:242–246. https://doi.org/10.1016/j.matdes.2014.02.038
33. Song Y, Li Y, Song W, Yee K, Lee KY, Tagarielli VL (2017) Measurements of the mechanical response of unidirectional 3D-printed PLA. Mater Des 123:154–164. https://doi.org/10.1016/j.matdes.2017.03.051
34. Sekaran JJG, Pragadish N, Valsakumari MK, Ravikumar S (2023) Characterization of fused deposition modeling components fabricated at different print orientations. Eng Res Exp 5:2. https://doi.org/10.1088/2631-8695/accad0
35. Sales E, Kwok TH, Chen Y (2021) Function-aware slicing using principal stress line for toolpath planning in additive manufacturing. J Manuf Process 64:1420–1433. https://doi.org/10.1016/j.jmapro.2021.02.050
36. Tam KMM, Mueller CT (2017) Additive manufacturing along principal stress lines. 3D Print Addit Manuf 4(2):63–81. https://doi.org/10.1089/3dp.2017.0001
37. Wang Z, Li J, Wu W, Zhang D, Yu N (2021) Multitemperature parameter optimization for fused deposition modeling based on response surface methodology. AIP Adv 11:5. https://doi.org/10.1063/5.0049357
38. Sandanamsamy L, Harun WSW, Ishak I, Romlay FRM, Kadirgama K, Ramasamy D, Idris SRA, Tsumori F (2022) A comprehensive review on fused deposition modelling of polylactic acid. Progr Addit Manuf. https://doi.org/10.1007/s40964-022-00356-w
39. Behzadnasab M, Yousefi AA, Ebrahimibagha D, Nasiri F (2020) Effects of processing conditions on mechanical properties of PLA printed parts. Rapid Prototyp J 26(2):381–389. https://doi.org/10.1108/RPJ-02-2019-0048
40. Hsueh MH, Lai CJ, Wang SH, Zeng YS, Hsieh CH, Pan CY, Huang WC (2021) Effect of printing parameters on the thermal and mechanical properties of 3d-printed pla and petg, using fused deposition modeling. Polymers 13:11. https://doi.org/10.3390/polym13111758
41. Wang S, Ma Y, Deng Z, Zhang S, Cai J (2020) Effects of fused deposition modeling process parameters on tensile, dynamic mechanical properties of 3D printed polylactic acid materials. Polym Testing 86:106483. https://doi.org/10.1016/j.polymertesting.2020.106483
42. Maguluri N, Suresh G, Rao KV (2021) Assessing the effect of FDM processing parameters on mechanical properties of PLA parts using Taguchi method. J Thermoplast Compos Mater 2:2. https://doi.org/10.1177/08927057211053036
43. Tian X, Liu T, Yang C, Wang Q, Li D (2016) Interface and performance of 3D printed continuous carbon fiber reinforced PLA composites. Compos A Appl Sci Manuf 88:198–205. https://doi.org/10.1016/j.compositesa.2016.05.032
44. Akhoundi B, Nabipour M, Hajami F, Shakoori D (2020) An experimental study of nozzle temperature and heat treatment (annealing) effects on mechanical properties of high-temperature polylactic acid in fused deposition modeling. Polym Eng Sci 60(5):979–987. https://doi.org/10.1002/pen.25353
45. Gao X, Qi S, Kuang X, Su Y, Li J, Wang D (2021) Fused filament fabrication of polymer materials: a review of interlayer bond. Addit Manuf 37(2):101658. https://doi.org/10.1016/j.addma.2020.101658
46. Bian YH, Yu G, Zhao X, Li SX, He XL, Tian CX, Li ZY (2022) Exit morphology and mechanical property of FDM printed PLA: influence of hot melt extrusion process. Adv Manuf. https://doi.org/10.1007/s40436-022-00405-1
47. Peng F, Vogt BD, Cakmak M (2018) Complex flow and temperature history during melt extrusion in material extrusion additive manufacturing. Addit Manuf 22:197–206. https://doi.org/10.1016/j.addma.2018.05.015
48. Das A, McIlroy C, Bortner MJ (2021) Advances in modeling transport phenomena in material-extrusion additive manufacturing: coupling momentum, heat, and mass transfer. Springer, Berlin. https://doi.org/10.1007/s40964-020-00137-3
49. Mackay ME (2018) The importance of rheological behavior in the additive manufacturing technique material extrusion. J Rheol 62(6):1549–1561. https://doi.org/10.1122/1.5037687
50. Phan DD, Swain ZR, Mackay ME (2018) Rheological and heat transfer effects in fused filament fabrication. J Rheol 62(5):1097–1107. https://doi.org/10.1122/1.5022982
51. Ge T, Pierce F, Perahia D, Grest GS, Robbins MO (2013) Molecular dynamics simulations of polymer welding: strength from interfacial entanglements. Phys Rev Lett 110(9):1–5. https://doi.org/10.1103/PhysRevLett.110.098301
52. McIlroy C, Olmsted PD (2017) Disentanglement effects on welding behaviour of polymer melts during the fused-filament-fabrication method for additive manufacturing. Polymer 123, 376–391. arXiv:1703.09295. https://doi.org/10.1016/j.polymer.2017.06.051
53. Das A, Gilmer EL, Biria S, Bortner MJ (2021) Importance of polymer rheology on material extrusion additive manufacturing: correlating process physics to print properties. Am Chem Soc. https://doi.org/10.1021/acsapm.0c01228
54. Das A, Riet JA, Bortner MJ, McIlroy C (2022) Rheology, crystallization, and process conditions: the effect on interlayer properties in three-dimensional printing. Phys Fluids 34:12. https://doi.org/10.1063/5.0128660
55. Ai JR, Vogt BD (2022) Size and print path effects on mechanical properties of material extrusion 3D printed plastics. Progr Addi Manuf 7(5):1009–1021. https://doi.org/10.1007/s40964-022-00275-w
56. Van de Voorde B, Katalagarianakis A, Huysman S, Toncheva A, Raquez JM, Duretek I, Holzer C, Cardon L, Bernaerts KV, Van Hemelrijck D, Pyl L (2022) Effect of extrusion and fused filament fabrication processing parameters of recycled poly(ethylene terephthalate) on the crystallinity and mechanical properties. Addit Manuf 50:102518. https://doi.org/10.1016/j.addma.2021.102518
57. Mahmoud Y, Manoochehri S (2021) In-situ Temperature Monitoring of ABS During Fused Filament Fabrication (FFF) Process

with Varying Process Parameters. In: Proceedings of the ASME 2021 International Design Engineering Technical Conferences and Computers and Information in Engineering Conference IDETC-CIE2021 August 17-19, 2021, Virtual, Online DETC2021-69813, pp. 1–10
58. Lee CY, Liu CY (2018) The influence of forced-air cooling on a 3D printed PLA part manufactured by fused filament fabrication. Addit Manuf 25:196–203. https://doi.org/10.1016/j.addma.2018.11.012
59. Kuznetsov VE, Solonin AN, Tavitov A, Urzhumtsev O, Vakulik A (2020) Increasing strength of FFF three-dimensional printed parts by influencing on temperature-related parameters of the process. Rapid Prototyp J 26(1):107–121. https://doi.org/10.1108/RPJ-01-2019-0017
60. Roy M, Yavari R, Zhou C, Wodo O, Rao P (2019) Prediction and experimental validation of part thermal history in the fused filament fabrication additive manufacturing process. J Manuf Sci Eng Trans ASME. https://doi.org/10.1115/1.4045056
61. Owens JT, Das A, Bortner MJ (2022) Accelerating heat transfer modeling in material extrusion additive manufacturing: from desktop to big area. Addit Manuf 55:102853. https://doi.org/10.1016/j.addma.2022.102853
62. ISO EN (2012) 527-2. Plastics-Determination of Tensile Properties-Part 2: Test Conditions for Moulding and Extrusion Plastics. Organization of Standardization: Geneva, Switzerland
63. Schröffer A, Prša J, Irlinger F, Lüth TC (2018) A novel building strategy to reduce warpage in droplet-based additive manufacturing of semi-crystalline polymers. 2018 IEEE International Conference on Robotics and Biomimetics, ROBIO 2018, 1894–1899. https://doi.org/10.1109/ROBIO.2018.8665054
64. Bernardez LD, Campana G, Mele M, Sanguineti J, Sandre C (2022) Effects of infill patterns on part performances and energy consumption in acrylonitrile butadiene styrene fused filament fabrication via industrial - grade machine. Progr Addit Manuf. https://doi.org/10.1007/s40964-022-00316-4
65. Montgomery DC (2013) Design and analysis of experiments, 8th Edition, p. 757. https://doi.org/10.1198/tech.2006.s372
66. Hanon MM, Marczis R, Zsidai L (2021) Influence of the 3D printing process settings on tensile strength of PLA and HT-PLA. Period Polytech Mech Eng 65(1):38–46. https://doi.org/10.3311/PPme.13683
67. Gilmer EL, Anderegg D, Gardner JM, Sauti G, Siochi EJ, McKnight SH, Dillard DA, McIlroy C, Bortner MJ (2021) Temperature, diffusion, and stress modeling in filament extrusion additive manufacturing of polyetherimide: an examination of the influence of processing parameters and importance of modeling assumptions. Addit Manuf 48:102412. https://doi.org/10.1016/j.addma.2021.102412
68. Tan WS, Tanoto YY, Jonoadji N, Christian AA (2021) The effect of cooling and temperature in 3D printing process with fused deposition modelling technology on the mechanical properties with polylactic acid recycled material. Int Rev Eng 15(12):615–621. https://doi.org/10.15866/ireme.v15i12.21573
69. Zhang X, Chen L, Mulholland T, Osswald TA (2019) Effects of raster angle on the mechanical properties of PLA and Al/PLA composite part produced by fused deposition modeling. Polym Adv Technol 30(8):2122–2135. https://doi.org/10.1002/pat.4645